

A Landau-Squire Nanojet: Supplementary Information

Nadanai Laohakunakorn,^{†,||} Benjamin Gollnick,^{‡,||} Fernando Moreno-Herrero,[‡]
Dirk G. A. L. Aarts,[¶] Roel P. A. Dullens,[¶] Sandip Ghosal,[§] and Ulrich F. Keyser^{*,†}

*Cavendish Laboratory, University of Cambridge, Cambridge CB3 0HE, United Kingdom,
Centro Nacional de Biotecnología, CSIC, Darwin 3, Campus de Cantoblanco, 28049 Madrid,
Spain,*

*Department of Chemistry, Physical and Theoretical Chemistry Laboratory, University of Oxford,
South Parks Road, Oxford OX1 3QZ, United Kingdom, and*

*Department of Mechanical Engineering & (by courtesy) Engineering Sciences and Applied
Mathematics, Northwestern University, Evanston Illinois 60208, United States*

E-mail: ufk20@cam.ac.uk

*To whom correspondence should be addressed

[†]University of Cambridge

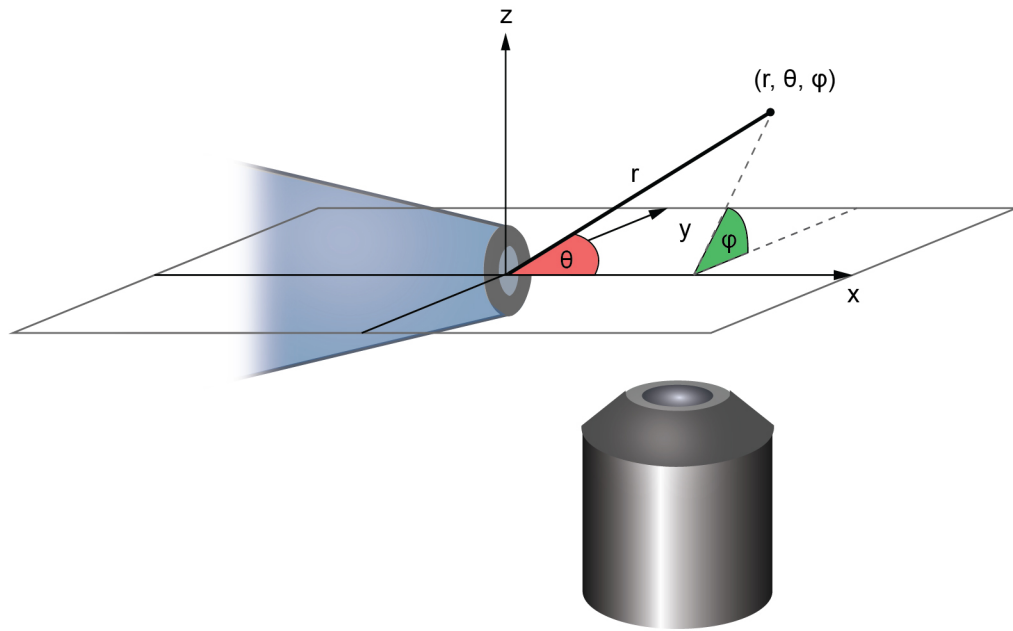
[‡]CSIC

[¶]University of Oxford

[§]Northwestern University

^{||}These authors contributed equally to the work.

Supplementary Figure S1

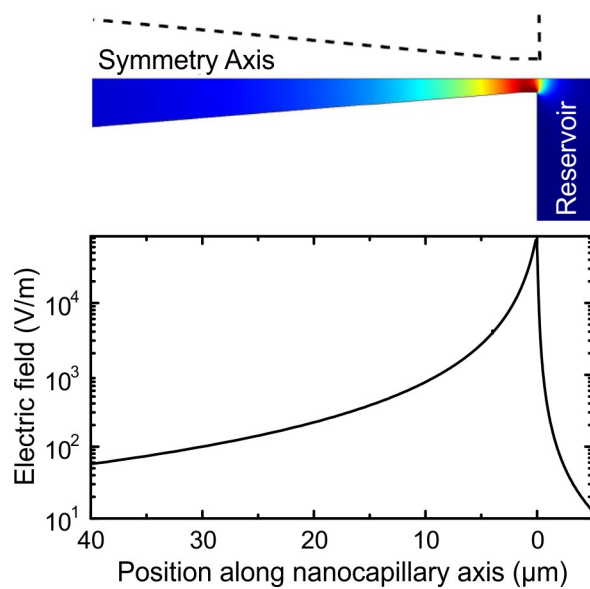


The coordinate system. The coordinate system used is sketched here. The origin is located at the pore. The x -axis is along the pore axis directed into the outlet reservoir and the z -axis is parallel to the optic axis of the microscope. All reported measurements are in the xy -plane ($z = 0$). The polar angle θ of the spherical polar system (r, θ, ϕ) is measured from the x -axis. Thus, the vorticity vector is always in the $\hat{\phi}$ direction, which corresponds to the directions \hat{z} (if $y > 0$) or $-\hat{z}$ (if $y < 0$) for measurements in the xy -plane.

Supplementary Movie S2

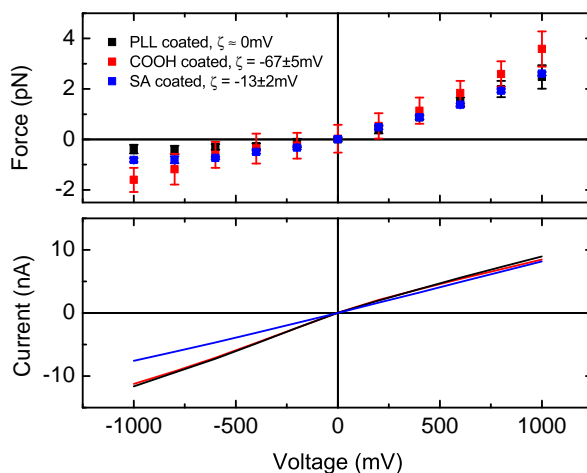
A rotating $2\ \mu\text{m}$ colloidal particle. This video shows three transverse scans: during the first scan, the voltage inside the pore is +1V, and the particle rotation is consistent with an outflow from the capillary. During the second scan, the voltage inside the pore has switched to -1V, and the rotation direction is in the opposite sense compared to the first scan. The third scan is a control carried out at 0V, and no rotation is observed.

Supplementary Figure S3



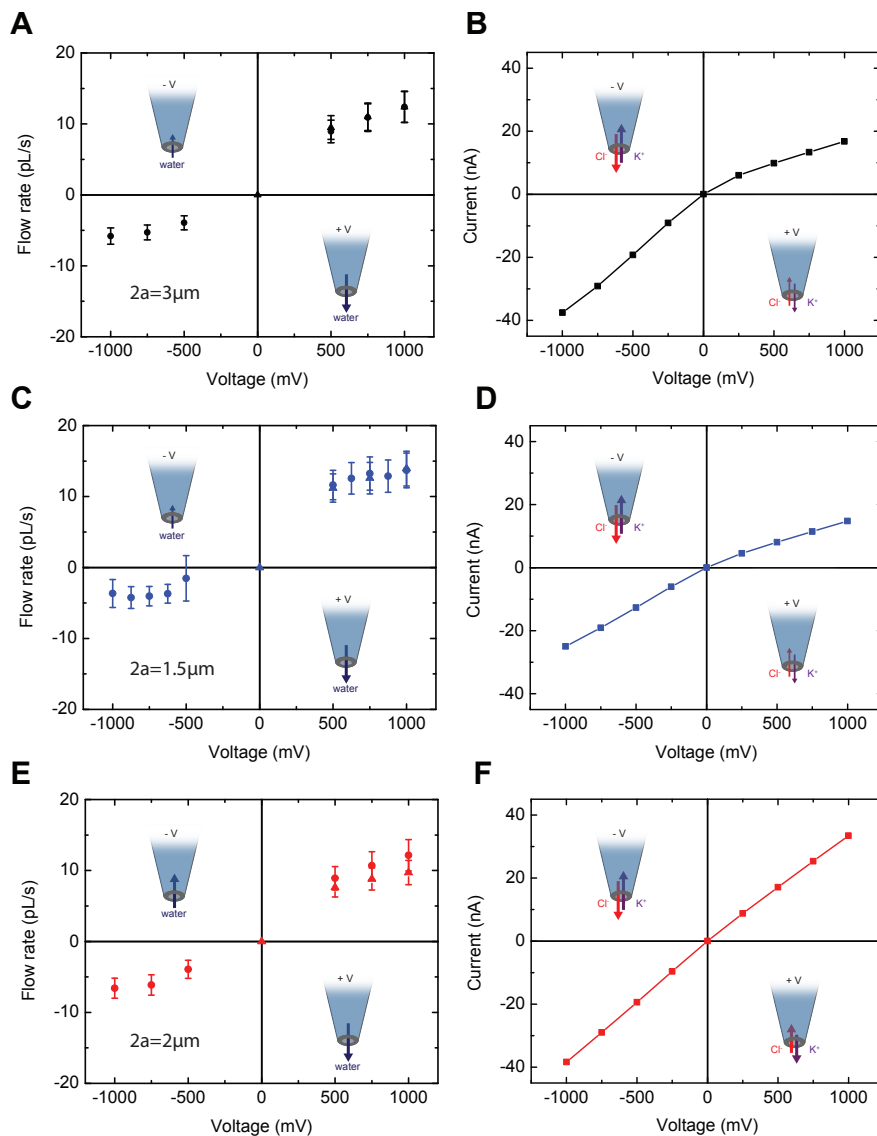
The electric field within the vicinity of the pore. The electric field within the vicinity of a 150 nm nanopore was determined using a finite-element method.² The electric field strength on-axis is shown in the graph, and a two dimensional representation is shown above; colours indicate the field strength. The applied voltage is +100 mV, and the salt concentration 20 mM. It is seen that the electric field drops to under 100 V/m within the first few microns outside the pore.

Supplementary Figure S4



The effect of changing colloidal surface charge. Here we show the force on a particle located on the pore axis at a fixed distance ($x = 2 \pm 0.3 \mu\text{m}$) from the tip as the voltage is varied. The three data sets were taken in three different pores but of almost identical size; the current-voltage graph gives an indication of the size variation. The black data set represents polystyrene particles with poly-L-lysine (PLL) coating; red represents carboxylated polystyrene particles, and blue represents streptavidin-coated polystyrene particles. All the particles are $2 \mu\text{m}$ in diameter. The different coatings result in different surface charges on the particles, which lead to different zeta potentials when measured in a commercial light scattering machine (Zetasizer, Malvern Instruments). The electric force is expected to scale proportionally to the zeta potential of the particle. However, the measured force is almost independent of the zeta potential. Thus, these measurements indicate that the electric force on the particle at distances of the order of $2 \mu\text{m}$ is much smaller than the non-electric force; in this case, the hydrodynamic drag due to the jet.

Supplementary Figure S5



Flow measurements for different particle sizes. Here we show the flow and ionic current as a function of voltage from three different data sets. Data Set 1 (Panels A,B): colloid diameter $3\ \mu\text{m}$, Data Set 2 (Panels C,D): colloid diameter $1.5\ \mu\text{m}$ and Data Set 3 (Panels E,F): colloid diameter $2\ \mu\text{m}$. Each set of measurements was performed with a new capillary but prepared using the same protocol (Data set 1 and 3 used the same capillary but the measurements were done at different times). The pore radii are all expected to be in the range $74 \pm 13\ \text{nm}$, based on SEM measurements

on a similarly prepared batch of capillaries. On the flow-voltage plots, circles indicate flow rates determined from rotation measurements, while triangles correspond to force measurements. Both methods agree within error. Despite the slight variability in pore size, geometry and buffer composition (evident from the I-V curves), flow rates obtained are of similar magnitude regardless of the size of the colloid used for measurement.

Supplementary Table S6

Data set	Colloid diameter (μm)	Flow rectification α_Q	Current rectification α_I
1	3	2.13	0.45
2	2	1.66	0.87
3	1.5	3.83	0.59

Quantitative measure of flow and current rectification. This table uses the data shown in Supplementary Figure S5. The flow rectification factor is defined as $\alpha_Q = |Q(1.0 \text{ V})/Q(-1.0 \text{ V})|$, and the corresponding current rectification factor is $\alpha_I = |I(1.0 \text{ V})/I(-1.0 \text{ V})|$. It is seen that flow rectification behaves in the opposite sense to current rectification: $\alpha_Q > 1$ when $\alpha_I < 1$. The strength of the two effects seem to be correlated, that is, a pore that shows strong current-rectification also displays strong flow rectification properties.